Supporting Information

Rapid Hybrid Chemical Vapor Deposition for Efficient and Hysteresis-Free Perovskite Solar Modules with an Operation Lifetime Exceeding 800 Hours

Longbin Qiu †, Sisi He †, Zonghao Liu, Luis K. Ono, Dae-Yong Son, Yuqiang Liu, Guoqing Tong, Yabing Qi*

† L. Qiu and S. He contributed equally to this work.

Energy Materials and Surface Sciences Unit (EMSSU), Okinawa Institute of Science and Technology Graduate University (OIST), 1919-1 Tancha, Kunigami-gun, Onna-son, Okinawa 904-0495, Japan.

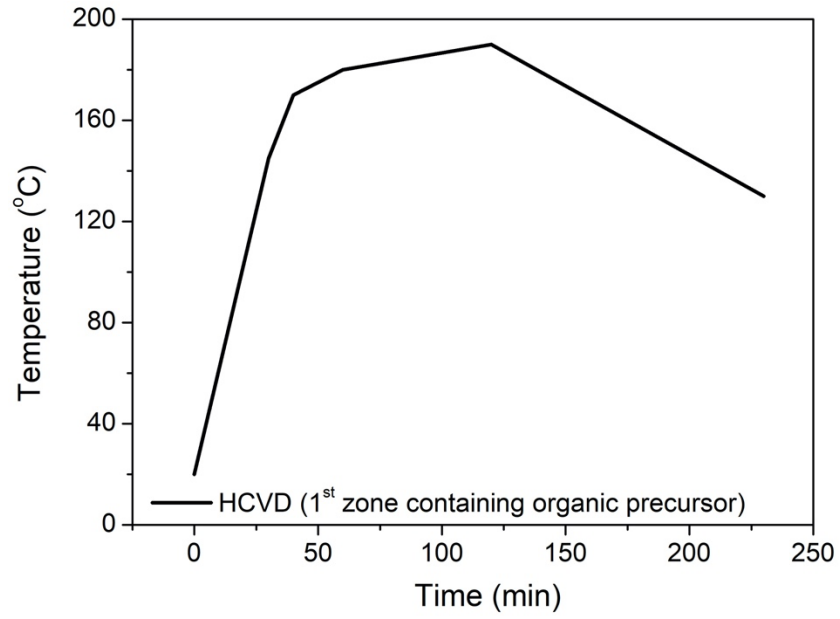***Corresponding author:** Yabing Qi, E-mail: Yabing.Qi@OIST.jp

Figure S1. Programed temperature profile as a function of time during the regular HCVD process for the heating zone containing the crucible with the organic precursor.
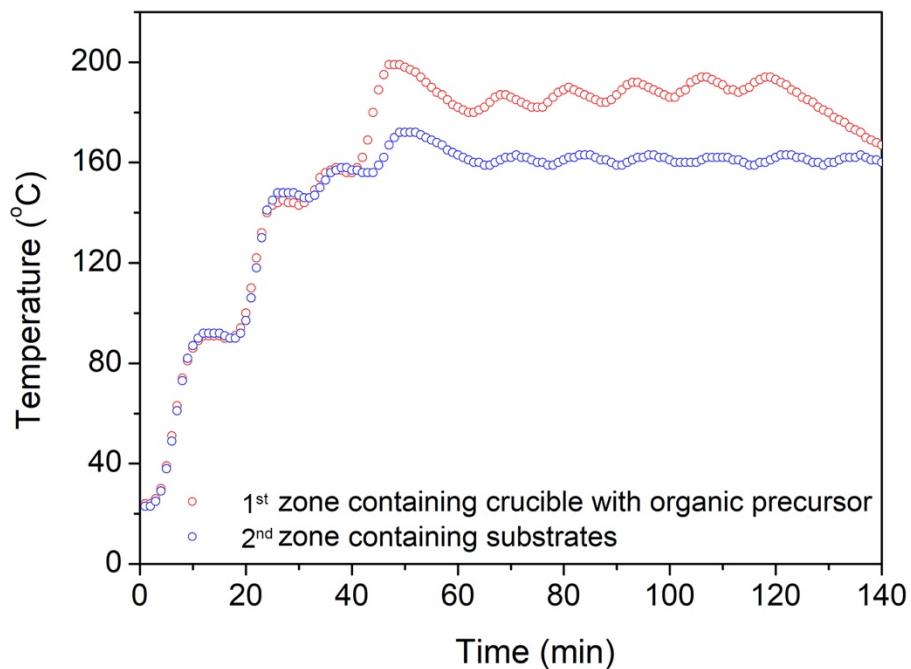
Figure S2. The recorded temperature profile for the regular HCVD method during the temperature ramping and deposition process for the 1st zone containing the crucible with the organic precursor and 2nd zone containing the substrates. Temperature fluctuation is observed during the temperature ramping and deposition processes. A slow ramping rate is used to minimize temperature overshooting with respect to the programmed temperature.
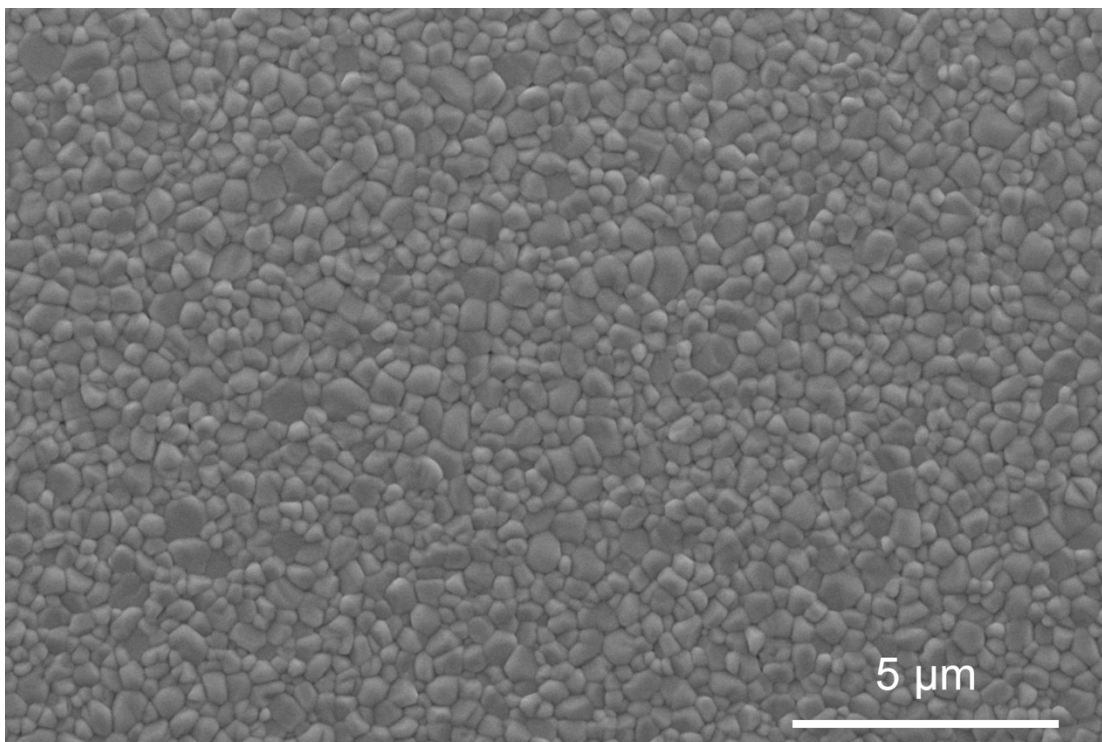
Figure S3. SEM micrograph showing the surface morphology of the RHCVD deposited $Cs_{0.1}FA_{0.9}PbI_3$ perovskite film across a relatively large area (20 μm × 13 μm).
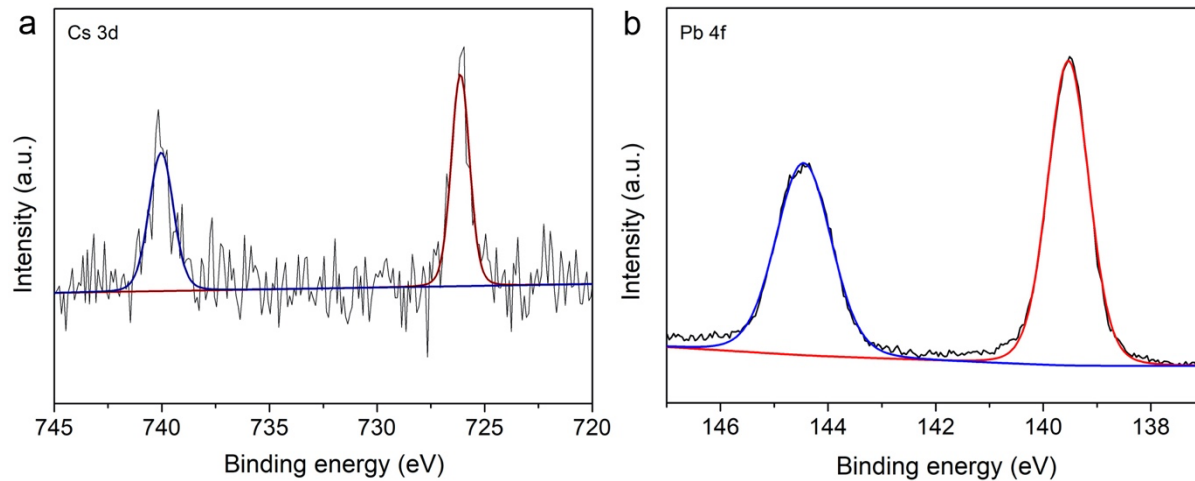
Figure S4. High resolution XPS spectra of **a.** Cs 3d and **b.** Pb 4f core levels confirming the incorporation of Cs cations into the perovskite films deposited by RHCVD.
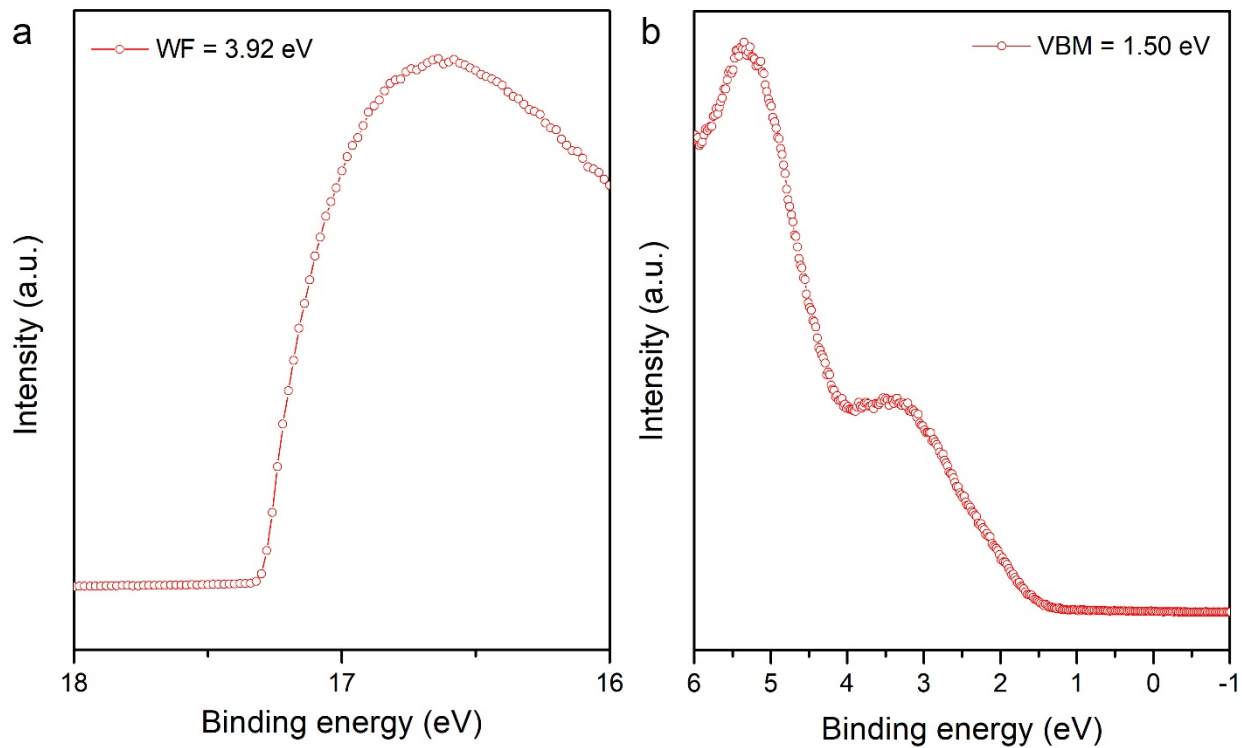
Figure S5. UPS spectra of the RHCVD deposited $Cs_{0.1}FA_{0.9}PbI_3$ perovskite layer. **a.** the work function of the perovskite layer is 3.92 eV. **b.** the valance band maximum for the perovskite layer is 1.50 eV below the Fermi level.
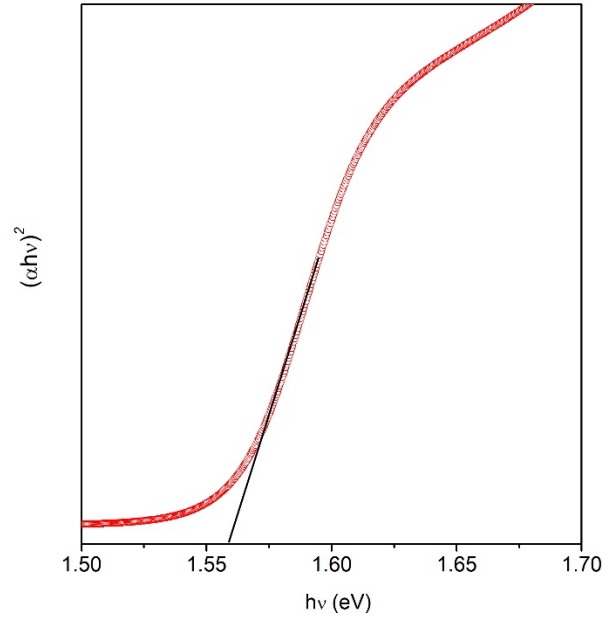
Figure S6. The optical band gap of the RHCVD deposited $Cs_{0.1}FA_{0.9}PbI_3$ perovskite film extracted from Tauc-plot is 1.56 eV.
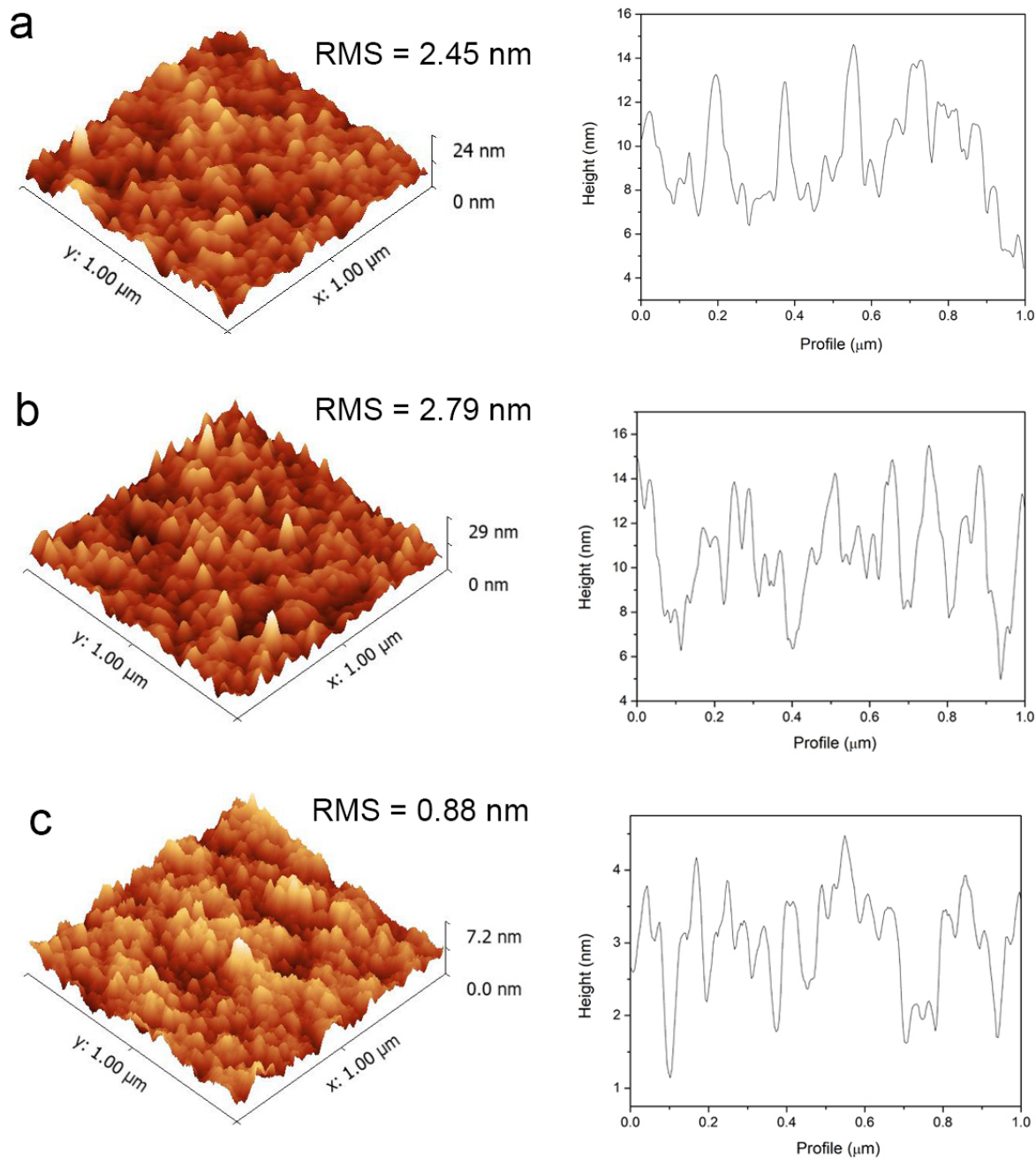
Figure S7. Atomic force microscopy images showing the surface morphology of **(a)** the bare ITO substrate, **(b)** sputter-deposited SnO_2 on the ITO substrate, and **(c)** spin coated SnO_2 nanocrystal film on the ITO substrate.
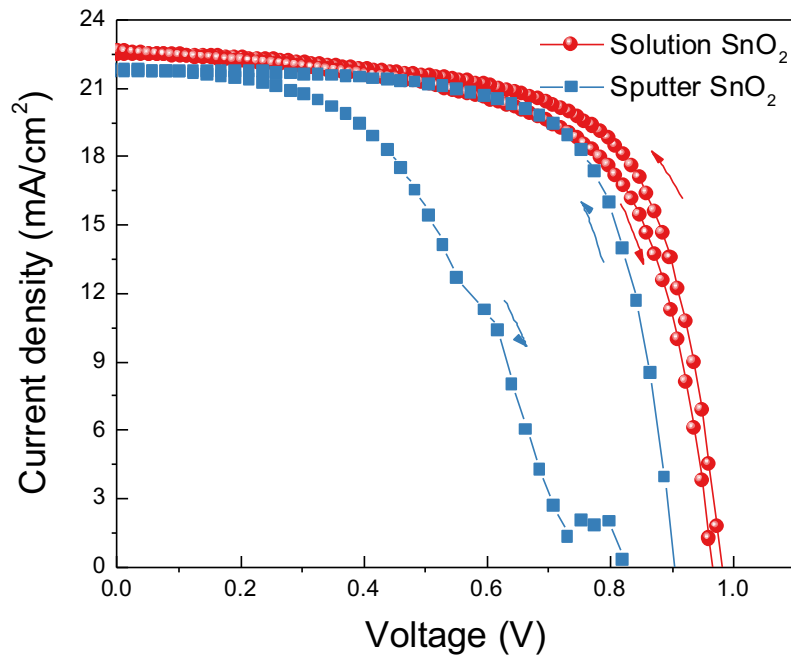
Figure S8. Current density-voltage curves of the PSCs based on the RHCVD-grown perovskite films deposited on the solution coated SnO_2 nanocrystal film and the sputter-deposited amorphous SnO_2 film, respectively. The reverse scan and forward scan PCE for the PSC based on the SnO_2 ETL prepared from the SnO_2 nanocrystals solutions are 15.0% and 14.1%, respectively. The reverse scan and forward scan PCE for the perovskite solar cell based on the sputter-deposited SnO_2 ETL are 13.8% and 8.1%, respectively.
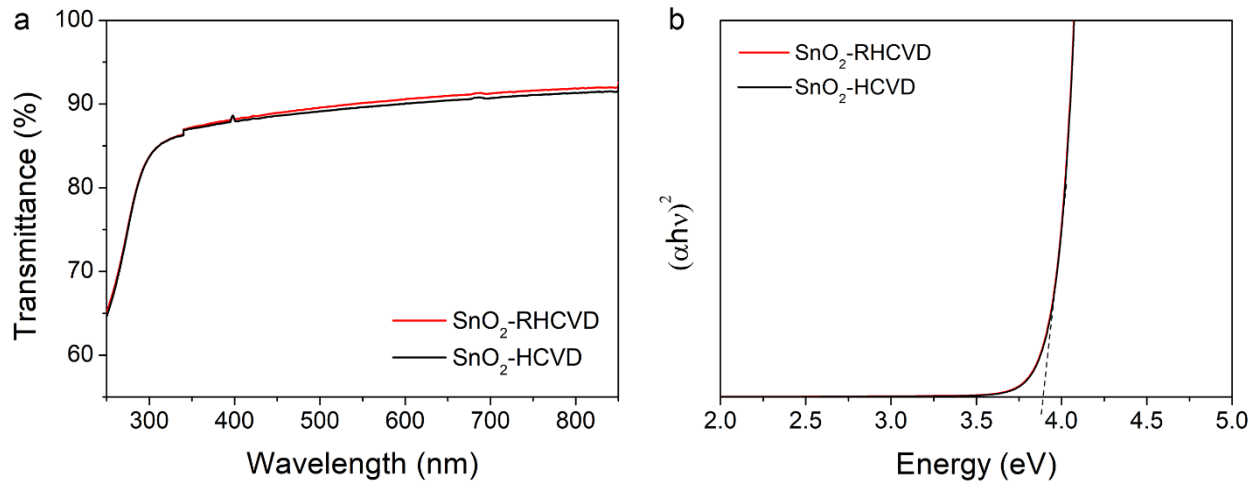
Figure S9. a) Transmittance spectra and **b)** Tauc-plot of the SnO_2 films after the RHCVD process and the regular HCVD process. The optical band gap of both films determined on the basis of the Tauc-plot is 3.85 eV.
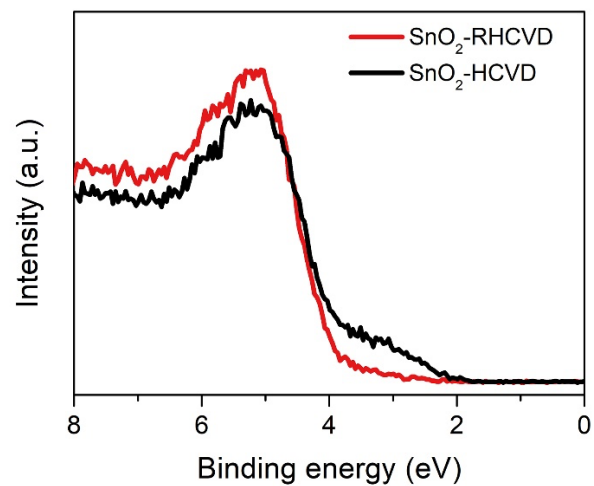
Figure S10. High resolution XPS valence features of the SnO$_2$ films based on the RHCVD process and the regular HCVD process.
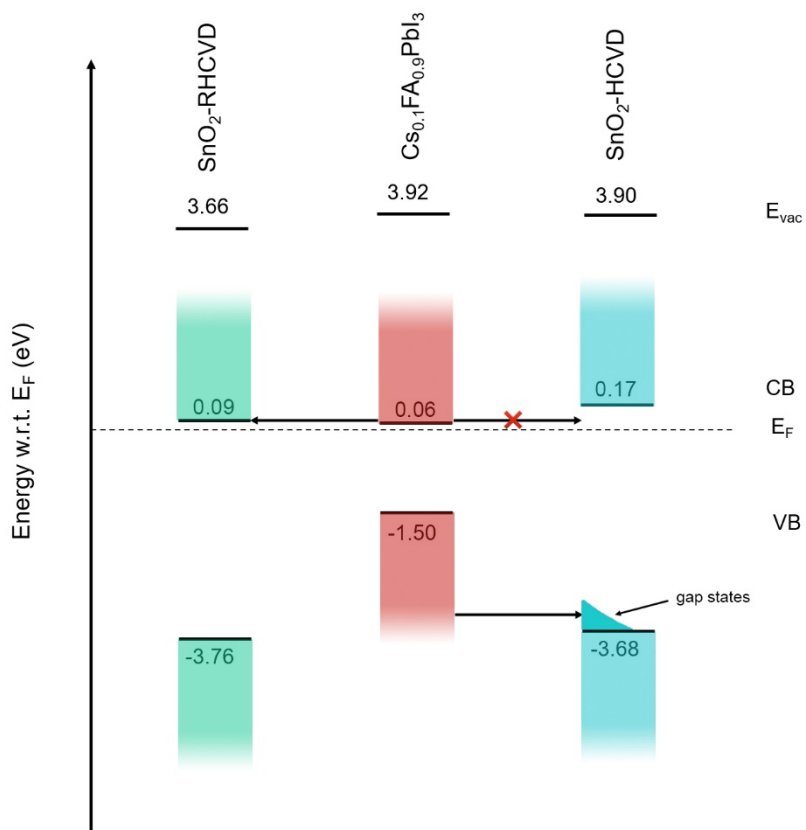
Figure S11. Energy level diagram of PSCs based on the vacuum annealed SnO_2 electron transport layer and the RHCVD grown $Cs_{0.1}FA_{0.9}PbI_3$ perovskite film.
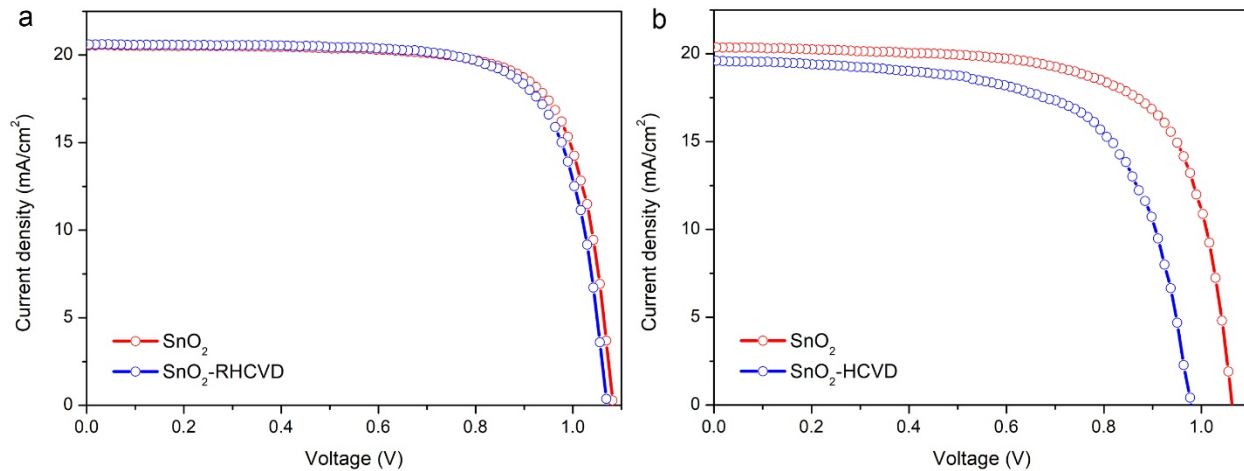
Figure S12. PSCs based on the spin coated perovskite layer on the nano-crystal SnO$_2$ layer **a)** with and without the RHCVD process and **b)** with and without the regular HCVD process.
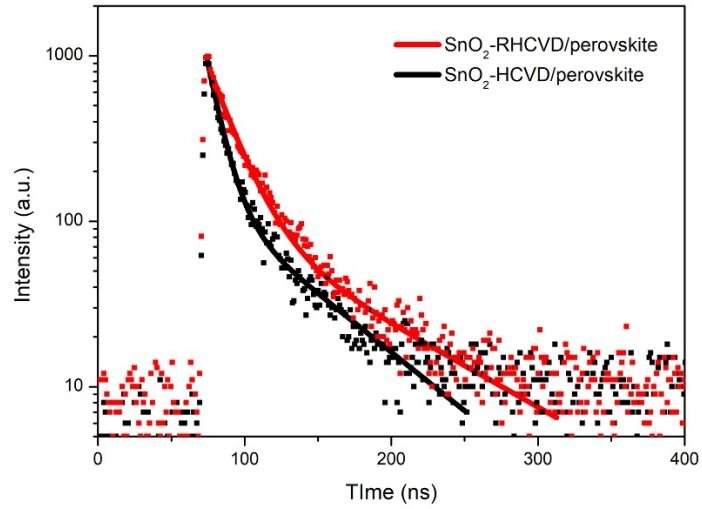
Figure S13. Time-resolved photoluminescence (TRPL) spectra of the solution coated CH$_3$NH$_3$PbI$_3$ film on the SnO$_2$ film after treatment of the RHCVD process and the regular HCVD process, respectively.
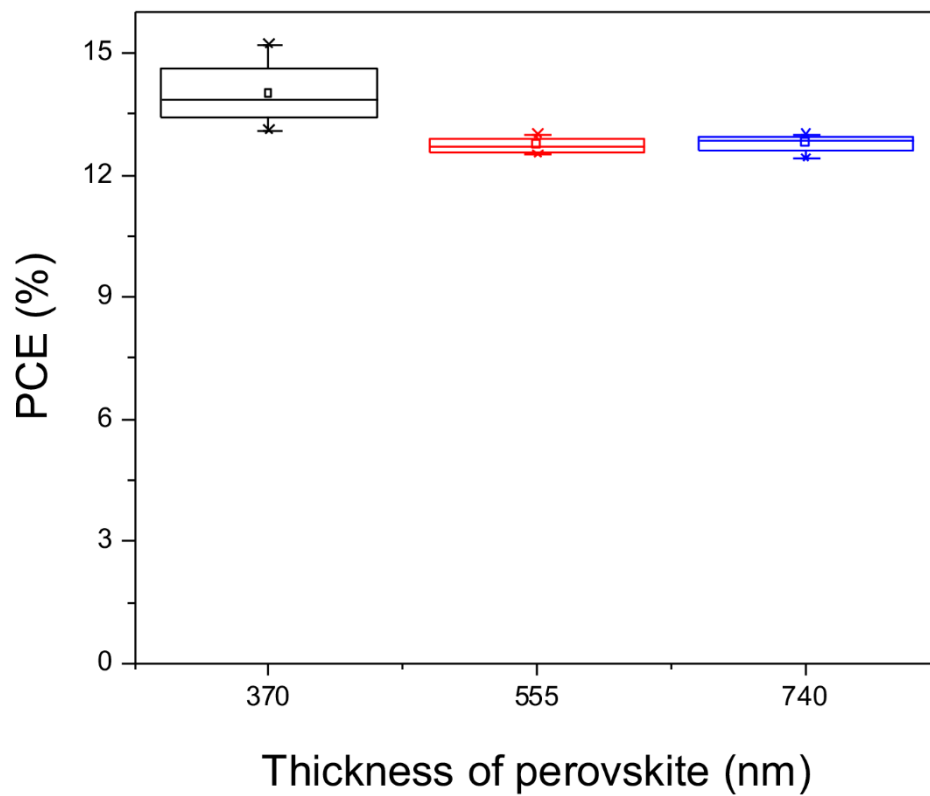
Figure S14. PCE as a function of the thickness of the deposited perovskite layer for RHCVD based PSCs.
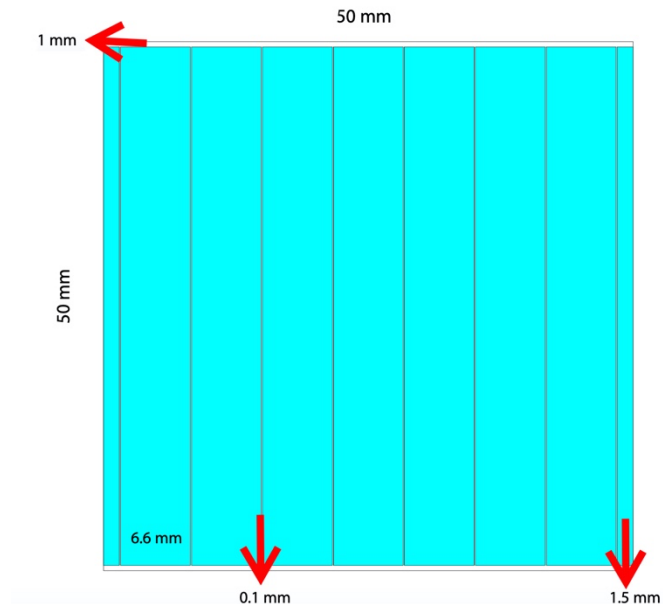
Figure S15. The schematic drawing showing the 5 cm × 5 cm substrate design for the PSM fabrication.

Table S1. The difference of Jsc values between the J-V curves and EQE curves.

Process	$J_{SC, \text{J-V}}$ (mA/cm^2)	$J_{SC, \text{EQE}}$ (mA/cm^2)	Difference (%)
RHCVD	22.3	21.2	4.93
HCVD	18.8	18.0	4.26

The difference is calculated as 1 - ($J_{SC, \text{EQE}}/J_{SC, \text{J-V}}$)

Table S2. TRPL results for $CH_3NH_3PbI_3$ on the SnO_2 films after the RHCVD process and the regular HCVD process.

Electron transport layer	τ_1 (ns)	τ_2 (ns)
SnO_2-RHCVD	17.8	87.9
SnO_2-HCVD	10.9	73.4

Table S3. Summary and comparison of the PSCs and PSMs fabricated by the typical solution coating process, regular HCVD as well as RHCVD. For the module area, [aa] means active area, and [da] means designated area. The hysteresis is defined as: HI = hysteresis index = $(\text{PCE}_{reverse} - \text{PCE}_{forward})/\text{PCE}_{reverse}$.

Perovskite	Coating method	Cell PCE (%)	hysteresis	Processing time (h)	Module (cm^2)	Module PCE (%)	Stability (h)	Ref
$(FAPbI_3)_{0.95}(MAPbBr_3)_{0.05}$	Spin coating	23.3	0.099	0.17	24.97[da]	17.1	>1370	S1
$MAPbI_3$	Doctor blading	21.3	0.006	~ 0.3	63.7[da]	16.4	N/A	S2
$MAPbI_{3-x}Cl_x$	Slot-die coating	16.8	N/A	0.25	151.9[aa]	10.6	N/A	S3
$(HOOC(CH_2)_4NH_3)_2PbI_4/CH_3NH_3PbI_3$	Screen printing	11.9	0.12	1	46.7[aa]	10.1	>10000	S4
$MAPbI_3$	HCVD	14.99	N/A	2	8.4[aa]	6.22	N/A	S5-6
$FAPbI_3$	HCVD	12.5	N/A	1	NA	7.7	N/A	S7
$MAPbI_3$	HCVD	15.6	N/A	1	8.8[aa]	9.5	N/A	S8
$Cs_xFA_{1-x}PbI_{3-y}Br_y$	HCVD	17.29	0.05	> 0.5	41.25[aa]	12.24	200	S9
$Cs_{0.07}FA_{0.93}PbI_3$	HCVD	16.6	0.13	3.5	12[aa]	14.6	N/A	S10
$Cs_{0.1}FA_{0.9}PbI_{2.9}Br_{0.1}$	HCVD	13.3	0.16	3.5	91.8[da]	9.34	500	S11
$FAPbIBr$	HCVD	15.6	0.08	3.5	12[aa]	14.7	388	S12
$Cs_{0.1}FA_{0.9}PbI_3$	RHCVD	15.5	0.09	~ 0.2	22.4[da]	12.3	> 800	This work

References:

[S1]   E. H. Jung, N. J. Jeon, E. Y. Park, C. S. Moon, T. J. Shin, T. Y. Yang, J. H. Noh & J. Seo. Nature 2019, 567, 511-515.

[S2]   Y. Deng, C. H. Van Brackle, X. Dai, J. Zhao, B. Chen & J. Huang. Sci. Adv. 2019, 5, eaax7537.

[S3]   F. Di Giacomo, S. Shanmugam, H. Fledderus, B. J. Bruijnaers, W. J. H. Verhees, M. S. Dorenkamper, S. C. Veenstra, W. Qiu, R. Gehlhaar, T. Merckx, T. Aernouts, R. Andriessen & Y. Galagan. Solar Energy Materials and Solar Cells 2018, 181, 53-59.

[S4]   G. Grancini, C. Roldan-Carmona, I. Zimmermann, E. Mosconi, X. Lee, D. Martineau, S. Narbey, F. Oswald, F. De Angelis, M. Graetzel & M. K. Nazeeruddin. Nat. Commun. 2017, 8, 15684.

[S5]   P.-S. Shen, J.-S. Chen, Y.-H. Chiang, M.-H. Li, T.-F. Guo, P. Chen, Adv. Mater. Interfaces 2016, 3, 1500849.

[S6]   M. Li, P. Shen, J. Chen, Y. Chiang, P. Chen, T. Guo, in *2016 23rd International Workshop on Active-Matrix Flatpanel Displays and Devices (AM-FPD)*, **2016**, pp. 256-257.

[S7]   M. R. Leyden, M. V. Lee, S. R. Raga, Y. B. Qi, J. Mater. Chem. A 2015, 3, 16097-16103.

[S8]   M. R. Leyden, Y. Jiang, Y. B. Qi, J. Mater. Chem. A 2016, 4, 13125-13132.

[S9]   L. Luo, Y. Zhang, N. Chai, X. Deng, J. Zhong, F. Huang, Y. Peng, Z. Ku, Y.-B. Cheng, J. Mater. Chem. A 2018, 6, 21143-21148.

[S10]   Y. Jiang, M. R. Leyden, L. Qiu, S. Wang, L. K. Ono, Z. Wu, E. J. Juarez-Perez, Y. B. Qi, Adv. Funct. Mater. 2018, 28, 1703835.

[S11]   L. Qiu, S. He, Y. Jiang, D.-Y. Son, L. K. Ono, Z. Liu, T. Kim, T. Bouloumis, S. Kazaoui, Y. B. Qi, J. Mater. Chem. A 2019, 7, 6920-6929.

[S12]   Y. Jiang, M. Remeika, Z. Hu, E. J. Juarez-Perez, L. Qiu, Z. Liu, T. Kim, L. K. Ono, D.-Y. Son, Z. Hawash, M. R. Leyden, Z. Wu, L. Meng, J. Hu, Y. B. Qi, Adv. Energy Mater. 2019, 9, 1803047.